Equilibrium theory of the hard sphere fluid and glasses in the metastable regime up to jamming. I. Thermodynamics

Ryan Jadrich and Kenneth S. Schweizer

Citation: The Journal of Chemical Physics **139**, 054501 (2013); doi: 10.1063/1.4816275
View online: http://dx.doi.org/10.1063/1.4816275
View Table of Contents: http://scitation.aip.org/content/aip/journal/jcp/139/5?ver=pdfcov
Published by the AIP Publishing

Equilibrium theory of the hard sphere fluid and glasses in the metastable regime up to jamming. I. Thermodynamics

Ryan Jadrich[1,2] and Kenneth S. Schweizer[1,2,3,a)]
[1]*Department of Chemistry, University of Illinois, Urbana, Illinois 61801, USA*
[2]*Frederick Seitz Materials Research Laboratory, University of Illinois, Urbana, Illinois 61801, USA*
[3]*Department of Materials Science, University of Illinois, Urbana, Illinois 61801, USA*

(Received 13 April 2013; accepted 7 July 2013; published online 1 August 2013)

We formulate and apply a non-replica equilibrium theory for the fluid-glass transition, glass thermodynamic properties, and jamming of hard spheres in three and all higher spatial dimensions. Numerical predictions for the zero complexity glass transition and jamming packing fractions, and a "densest" equilibrium glass, are made. The equilibrium glass equation of state is regarded as the practical continuation of its fluid analog up to jamming. The analysis provides a possible resolution to the inability of any fluid virial series re-summation based equation of state to capture jamming at a reasonable volume fraction. The numerical results are quantitatively compared with various simulation data for equilibrium hard sphere glasses in 3 to 12 dimensions. Although there are uncertainties in this comparison, the predicted zero complexity or configurational entropy and corresponding jamming packing fractions do agree well with two characteristic packing fractions deduced from the dynamic simulation data. The similarities and differences of our approach compared to the replica approach are discussed. The high dimensional scaling of the equilibrium glass transition and jamming volume fractions are also derived. The developments in this paper serve as input to Paper II [R. Jadrich and K. S. Schweizer, J. Chem. Phys. **139**, 054502 (2013)] that constructs a self-consistent integral equation theory of the 3-dimensional hard sphere pair structure, in real and Fourier space, in the metastable regime up to jamming. The latter is employed as input to a microscopic dynamical theory of single particle activated barrier hopping. [http://dx.doi.org/10.1063/1.4816275]

I. INTRODUCTION

A. Motivation

The venerable hard sphere system, in the thermodynamically stable fluid, over-compressed metastable fluid, and non-equilibrium amorphous solid regimes remains of significant interest with regards to understanding the structure and slow dynamics of amorphous materials. This interest has grown in recent years motivated by questions such as the nature of granular jamming[1] and glassy dynamics of very concentrated Brownian colloidal suspensions.[2–5] The hard sphere model continues to serve as a useful reference system for finite range soft repulsive fluids and thermal liquids.[6,7]

Historically, equilibrium theories of simple fluids have employed the Ornstein-Zernike integral equation with approximate closure relations.[8,9] Though highly developed below the freezing packing fraction, $\eta_f \approx 0.494$, such theories qualitatively fail in the metastable regime, and increasingly so as the jammed or "random close packing" (RCP) state at $\eta_{RCP} \approx 0.64$ is approached. The latter is not rigorously well-defined due to its nonequilibrium nature and non-unique jamming density.[10–13] This has led to the proposal of a unique "maximally randomly jammed" (MRJ) state.[1,13] However, the exact protocol dependence often seems of secondary order importance in practice,[1,14] and here we ignore any differences between RCP and MRJ.

There has been a flurry of recent theoretical work on hard sphere glass formation based on the idealized thermodynamic viewpoint of equilibrium mean field replica theory (RT), including a generalization to treat jammed monodisperse[15] and multicomponent hard sphere[16] fluids, as well as soft sphere systems.[17] RT predicts a fragmentation of the free energy landscape corresponding to the emergence of an extensive number of metastable states with finite complexity (analog of configurational entropy) at a packing fraction η_d. This phenomenon is not associated with a thermodynamic phase transition. Further densification results in a second order phase transition, also known as the Kauzmann entropy crisis, at η_K where the complexity vanishes and the compressibility changes discontinuously. Additional compaction eventually results in jamming at "glass close packing" (GCP), η_{GCP}, the *unique* maximally dense jammed amorphous glass packing attainable, which serves as an upper bound to η_{RCP} or η_{MRJ}[15] in the absence of crystallization. While the lack of crystallization is hard to precisely define, simulations[10,11,18,19] suggest there is a wide range of jamming densities (range increases with dimensionality) realizable without increased crystalline ordering, consistent with the replica theory view of glasses and jamming.[15] Older density functional theory (DFT)[20] and dynamic ideal mode coupling theory (MCT)[21] also predict localization transitions to a nonergodic amorphous solid at

a)kschweiz@illinois.edu

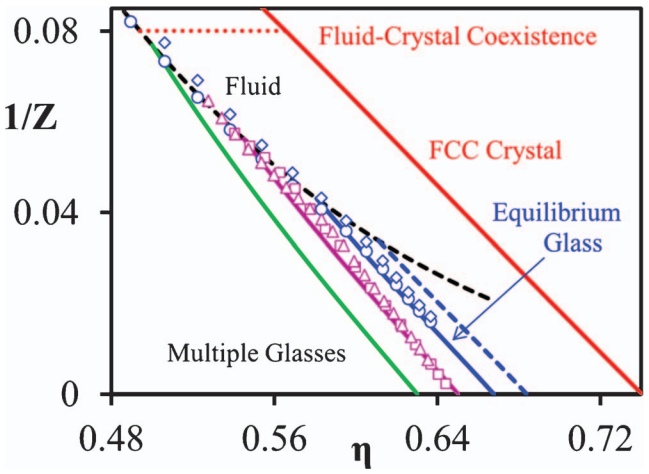

FIG. 1. Three-dimensional hard sphere fluid-crystal-glass phase diagram in the representation of inverse compressibility factor versus packing fraction. The stable fluid line (upper black dashed curve) was calculated using the accurate Kolafa EOS.[44] The four glass branches computed using our theory correspond to (left to right) $\eta_g = 0.50$, 0.545, and 0.581 (most realistic equilibrium glass) and 0.611 with increasing jamming density. Open purple triangles and squares correspond to the well-aged polydisperse hard sphere data of Hermes and Dijkstra[11] and mondisperse hard spheres of Speedy,[24] respectively. Open blue diamonds and spheres correspond to binary hard sphere simulation data of Odriozola and Berthier[23] and the corresponding inferred mondisperse data of Santos *et al.*,[50] respectively. The FCC crystal line was calculated using the accurate Speedy equation-of-state.[24]

the analog of η_d. Although RT, DFT, and MCT are similar in spirit, all are approximate mean field theories which make quantitatively different predictions for characteristic packing fractions, and in elevated dimensions appear to differ qualitatively.[15,18,20–22] More generally, the connection between the thermodynamic glass formation scenario and dynamic vitrification remains an intensely debated and controversial issue.

There have been many recent simulation studies aimed at trying to (approximately) identify signatures of an equilibrium thermodynamic glass transition in hard sphere systems.[10,11,18,23] This is a subtle task given that glass formation depends on simulation protocol and ultimately is limited by kinetic trapping into lower density nonequilibrium glass states. Figure 1 shows some results for the equation-of-state (EOS) in the representation of the inverse dimensionless compressibility factor, Z.[11,24] Distinguishing features are the apparent kink in the curve at high packing fractions which, in analogy with such a feature in the volume-temperature curve of thermal glass forming liquids, suggests the emergence of glassy metastable states on the simulation time scale, or "practical vitrification." The jamming point is deduced via extrapolation of $1/Z \to 0$ where the pressure diverges and compressibility vanishes.[1,10,11,18] Recent work has studied how these features evolve as the spatial dimension grows beyond three.[18] A caveat of high relevance to our present work is that uniquely relating characteristic packing fractions deduced from simulation to their theoretical counterparts, even in the putative low compaction rate limit, is fundamentally difficult and involves some ambiguity.

Our goal is to develop a new, rather simple, non-replica-based thermodynamic approach to glass formation. Though of interest in its own right, the *primary* motivation of the thermodynamic developments in this paper is to provide a theoretical foundation to create a new thermodynamically self-consistent integral equation theory of the pair structure of 3-dimensional metastable hard sphere fluids up to the jamming point that can reliably predict the extremely high wavevector correlations not easily extracted from simulation. The latter is the key input to the nonlinear Langevin equation dynamical theory of single particle activated hopping.[25,26] To place our approach in perspective, establish notation, and define our goals, we first review in Secs. I B and I C recent simulation and theory studies relevant to our work. Section I D outlines our approach. We emphasize that we are not advocating a literal interpretation of glass formation as an equilibrium phase transition. We also note that the higher dimensional generalization of (only) our thermodynamic theory is worked out and applied primarily due to the present interest in this topic in the statistical physics community, and also because it provides additional insight concerning the accuracy of our approach and its relation to replica theory.

B. Simulation studies

Examples of simulations of the inverse compressibility factor of hard spheres in 3-dimensions are shown in Figure 1, which are typically performed at a variable rate of dynamic compression, Γ. As long as the structural relaxation time is short enough, the measured EOS follows the equilibrium behavior which is accurately described by virial series re-summation expressions such as the Carnahan-Starling formula.[27–31] However, for a fixed compression rate, at a high enough η the EOS departs from the fluid form in a kink-like manner which operationally defines a compression-rate-dependent "glass transition" packing fraction, $\eta_g(\Gamma)$,[11,12,18] that grows with decreasing rate. The kink at $\eta_g(\Gamma)$ "looks" like a second order phase transition. At higher packing fractions, the pressure rapidly increases in a "free volume-like" inverse critical power law manner, and diverges at a *compression rate dependent* jamming volume fraction $\eta_j(\Gamma)$.[11,12,18] For each $\eta_g(\Gamma)$ there is a corresponding compression rate dependent jamming volume fraction, $\eta_j(\Gamma)$, and both increase with decreasing Γ.

Given this compression rate dependence, one can ask how can the glass and jamming transitions ever be treated from an equilibrium thermodynamic standpoint? Perhaps surprisingly, if crystallization is avoided, a limiting low (but nonzero) rate behavior has been demonstrated in the spirit of an extrapolated $\Gamma \to 0$ state, thereby allowing the deduction of $\eta_g(0) \equiv \eta_g(\Gamma \to 0)$ and $\eta_j(0) \equiv \eta_j(\Gamma \to 0)$ corresponding to a hypothetical equilibrium glass.[18] These two quantities define a *practical simulation* equilibrium glass transition which is the "densest" glass where the EOS first departs the fluid branch; a densest jammed state at $\eta_j(0)$ is deduced via a $1/Z \to 0$ extrapolation. However, in practice, the deduction of $\eta_g(0)$ and $\eta_j(0)$, and their theoretical interpretation, is subject to some uncertainty as further discussed in Sec. I C. Complementary static aging replica exchange Monte Carlo simulations[23] also suggest the existence an equilibrated densest glass. Hence, simulations can locate a continuum of

amorphous glass branches by varying the dynamic compression rate or extent of the aging of an initially prepared configuration. Higher density glasses correspond to longer aging periods or slower compressions. Physically, it is reasonable to believe that denser glasses have better defined thermodynamic properties because of slower aging and increased metastability. The most ideal realization corresponds to the hypothetical equilibrium glass branch. For excellent summaries of these phenomena we refer the reader to Refs. 15 and 18.

C. Thermodynamic mean field theories and connection to simulation

RT is a mean field thermodynamic approach based originally on one step replica symmetry breaking in infinite range spin glass models[32] that has been extended to homogeneous liquids to treat structural glasses that do not have quenched disorder.[15–17] Four characteristic packing fractions are predicted: two characteristic glass transitions, η_d and η_K, and two characteristic jamming transitions, η_{th} and η_{GCP}. The transition at η_d signifies the initial emergence of metastable glassy states, and corresponds to the lowest density or "threshold" glass with a jamming density at η_{th}. The emergence of glassy states is widely believed to be a dynamic crossover since, in reality, different amorphous packings are separated on the free energy landscape by finite, not infinite, barriers. Above η_d denser glass states exist up till the Kauzmann density, η_K, where the number of metastable states becomes sub-exponential in particle number. The glass state at η_K is the theoretical densest possible glass or *ideal glass*. The ideal glass jams at Glass Close Packing, η_{GCP}. Note that the ability to precisely define η_d and η_{th} is intimately related to use of the idealized mean field approximation.

Older DFT approaches to glass formation adopted a real space picture.[20] They predict localization and metastable amorphous states at η_d based on a free energy calculation. The resultant glass free energy is purely "vibrational" in the sense it only counts configurations associated with small displacements around one global amorphous configuration. In general, there is an exponential number of global amorphous configurations so when the glass free energy equals the fluid at higher packing fractions, the system is interpreted as trapped in a sub-exponential number of amorphous packings, also known as the entropy crisis, at η_K. Zamponi[33] has emphasized the limitations of DFT, especially its inability to truly count metastable states as a function of system size which implies a full thermodynamic treatment (e.g., calculation of complexity) is impossible. Ideal MCT is a dynamical approach for particle localization,[21] and although connections with DFT and RT have been discussed,[15,20] significant puzzles remain with regards to the level of equivalency.[15,18]

All three of the above theoretical approaches are approximate, in different ways, and built on a mean field picture of literal localization and/or thermodynamic glass "phases." The extent to which the scenarios they predict are valid is unclear, and the characteristic packing fractions below jamming are not truly well-defined.[15,18,22] Thus, how can one objectively deduce from simulation $\eta_K > \eta_d$ and $\eta_{GCP} > \eta_{th}$? At present, attempts to relate theory and simulation (even in the low compression rate limit) are somewhat unsettled. Theoretically, an ideal glass is the densest possible glass observable and would be obtained by infinitesimally slow compressions. In practice, the ideal glass is unobservable since the equilibration time diverges upon approaching η_K. From this logic, the simulation extrapolated quantities $\eta_g(0)$ and $\eta_j(0)$ correspond to η_K and η_{GCP}, respectively.[15] Some have suggested[18] that $\eta_g(0)$ and $\eta_j(0)$ may actually be closer to η_d and η_{th} depending on both the dimensionality and how the extrapolation is performed. High dimensionality is generally believed to promote an increase in barrier heights separating metsatable glassy states,[15,18] and hence practical simulation limitations would more likely yield $\eta_g(0) \cong \eta_d$. In the hypothetical $D \to \infty$ limit, η_d may become a rigorous transition if barrier heights diverge.[15] Additional ambiguity arises from choosing between extrapolation functional forms. Two theoretically motivated choices assume convergence to $\Gamma = 0$ based on either a power law form,[18] Γ^α, or a Volger-Fulcher-Tammann (VFT) form,[11,15,18] $1/|\log \Gamma|$ where α is a constant. The power law form is believed to extrapolate closer to η_d, and the VFT form to η_K. These two choices are also faced with uncertainty since for 4D hard spheres extrapolation to zero compression rate based on either power law or VFT forms results in similar values of $\eta_g(0) = 0.401$[18] and 0.409,[15] respectively, significantly smaller than the 4D replica theory Kauzmann transition at $\eta_K = 0.432$.

Definitive resolution of the above uncertainties is difficult and requires, at a minimum, a more precise knowledge of barrier heights separating metastable states. Alternatively, the direct evaluation of η_K by approximately counting the number of glass states would provide a useful comparison to $\eta_g(0)$. Recent simulation-based calculations of this type have been performed by Angelani and Foffi[34] for a binary 3D hard sphere mixture and by Torquato and co-workers for a binary hard disk mixture.[35] However, these methods are also subject to uncertainty associated with the non-unique definition of a glassy state and the validity of the extrapolation to η_K, as pointed out in Ref. 35. Given these many subtle issues, we will not insist on resolving the precise theoretical meaning of $\eta_g(0)$ and $\eta_j(0)$, but rather focus on building a theory that can predict η_K and η_{GCP}. Subject to the above caveats, these quantities will be compared to simulation power law extrapolated $\Gamma \to 0$ characteristic packing fractions[18] and also replica theory predictions for η_K and η_{GCP}.[15]

D. Our approach

We aim to predict the EOS and glass transition and jamming packing fractions of the metastable fluid glassy branches of hard sphere systems. Most importantly, we are interested in the possible equilibrium (densest) ideal glass that continues the fluid into the metastable regime since we are largely motivated to understand *equilibrium* glass-like dynamics in ultra-dense hard sphere fluids. Such a viewpoint is in analogy with the study of supercooled thermal liquid dynamics which remains equilibrated until a kinetic vitrification temperature is reached. The possible relevance of this view for hard spheres is supported by simulations, especially the replica exchange studies.[23] Broadly speaking, when referring to a glass, there

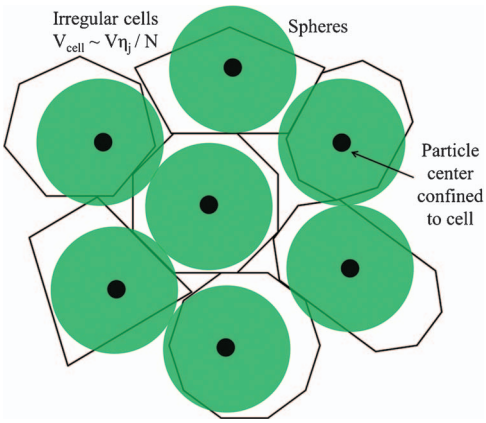

FIG. 2. Schematic of the cell model of a glass where particle centers are confined within the irregularly shaped Voronoi-like cells of fixed volume. Open space is present since the cells utilize a total volume of $V\eta_j$, where η_j corresponds to the jamming volume fraction of the particular glass.

are two possibilities: (i) multiple *non-equilibrium* glasses that depend on protocol, and (ii) one hypothetical uniquely defined maximally dense *equilibrium* glass.

We aim for a real space, local cell description of the configurational state of liquids and glasses at the level of individual particles, as indicated schematically in Figure 2. This is perhaps reminiscent of a DFT-like description or Voronoi tessellation.[20,36] However, we do not include Gaussian vibrations, but rather focus on the system-size-dependent thermodynamic complexity. Our approach is built on an idealized second order phase transition between a fluid and homogeneous glass at a characteristic packing fraction η_K, which upon further compression ultimately jams at η_{GCP}. We do not predict the analog of η_d in RT, DFT or MCT, the first emergence of metastable states and particle localization, which might be identified with the onset of applicability of the localized cell picture we adopt. Rather, we operationally introduce a nonuniversal glass transition packing fraction, η_g, that identifies when the EOS first does not follow the expected equilibrated fluid behavior. Though this quantity is compression rate dependent in simulation, it is not explicitly so in our thermodynamic theory.

The above ideas are specifically implemented by building on the scaled particle theory (SPT) approach of Baeyens and Verschelde (BV).[37] Multiple glassy branches exist with different amounts of complexity, Σ, which quantifies the number of glass states and vanishes at an equilibrium ideal glass transition at η_K. The calculated equilibrium glass EOS is envisioned as a *practical* continuation of the *equilibrium* fluid in the metastable regime up to the jamming point. Our results for characteristic packing fractions are tentatively compared to recent simulations in $D = 3$–12, and also replica theory.

Section II presents our theory for the EOS of glassy hard spheres; derivation details are given in the Appendix. We also derive the high dimensional scaling form for the equilibrium glass and jamming transition packing fractions. Section III presents calculations in 3-dimensions and compares to simulation. Numerical results beyond 3-dimensions, including the high dimensional limit, for the glass transition and jamming packing fractions, and their scaling forms, are presented in Sec. IV and compared to simulations, replica theory, MCT, and the best known bounds on the highest achievable jammed packing density.[38–40] A more general comparison of our approach with RT is given in Sec. V. The paper concludes with a discussion in Sec. VI. Paper II[55] formulates and applies a theory for pair structure building on the thermodynamic approach of the present article, and utilizes it to study single particle activated dynamics.

II. THEORY

We assume crystallization can be avoided in principle, and thus equilibrated amorphous phases can be studied up to jamming. Practical realization of this may require size polydispersity[41–43] or dimensionality higher than three,[12,18] but we believe the physics of putative monodisperse equilibrium amorphous systems is closely related to such systems. Such a perspective underlies RT and DFT descriptions of glassy hard spheres.

A. Fluid phase

The fluid EOS is well described by re-summed virial series expressions.[11,12,15,29–31] We define the *fluid* regime operationally as the packing fraction range below the approximate onset of free volume pressure growth near a glass transition packing fraction η_g. In simulation or experiment, η_g appears to be rather well-defined,[11,12,15,18] and we assume the crossover is sufficiently sharp that a cusp in the pressure (discontinuous jump of the compressibility) is a reasonable approximation and serves as a well-defined surrogate for our theoretical η_g. Multiple good fluid EOSs exist for hard spheres. We adopt the Kolafa form[44]

$$Z_{3,f}(\eta) \equiv \frac{1+\eta+\eta^2-2(\eta^3+\eta^4)/3}{(1-\eta)^3}, \tag{1}$$

where the subscript 3 indicates three dimensions and f denotes fluid. Equation (1) is marginally more accurate than the Carnahan-Starling (CS) formula,[27,28] though either would suffice for our purposes. In higher dimensions, we use the generalization of the CS form[15,18,28]

$$Z_{D,f}(\eta) \equiv 1 + 2^{D-1}\eta\frac{1-A_D\eta}{(1-\eta)^D}, \tag{2}$$

where A_D follows from the virial series coefficients,[28] or alternatively from fitting simulation results which we use for increased accuracy in 4 to 12 dimensions.[18]

B. Glass equation of state and formation

The glass EOS applies for all $\eta > \eta_g$ and is characterized by free volume pressure growth and eventual jamming at η_j.[10–12,15,18] We model a glass, by definition here composed of an extensive number of individual packing states, by building on the SPT result of Baeyens and BV,[37] which we have generalized to $D \geq 3$ in the Appendix. The compressibility

factor is given by

$$Z_{D,g}(\eta) \equiv \frac{1 + p_1\eta + p_2\eta^2}{(1-\eta)^2(1 + (p_1 - (2^{D-1} - 2))\eta)}, \quad (3)$$

where p_1 and p_2 are determined as described below and g denotes glass. The utility of Eq. (3) rests on it being derived from *exact* SPT criteria. For the 3D fluid, BV determined p_1 and p_2 from an exact hard sphere low density expansion of SPT correlation functions giving $p_1 = 1.2117\ldots$ and $p_2 = 1.4234\ldots$, which results in a fluid EOS that is practically identical to Eq. (1) or the CS EOS.[37] In principle, Eq. (3) could be systematically extended to include more parameters that can be chosen to enforce more exact constraints in the SPT framework, but eventually higher order correlation functions enter. Equation (3) can be tentatively interpreted as the best possible representation of a given amorphous state subject to enforcing only two thermodynamic constraints.

BV used Eq. (3) to describe a glass transition in a manner that is different than we develop here. They adopted a Cohen-Grest like[45] cell model picture, where glassy states composed of N hard spheres consist of two subsystems, G_1 and G_2, which are solid-like and fluid-like, respectively. The two subsystems occupy disconnected regions, and only the solid-like subsystem has a divergent pressure at jamming. BV further assumed: (i) G_1 and G_2 have the same density, (ii) the fluid free energy remains non-singular below the jamming packing fraction, (iii) G_1 is completely frozen and particles are distinguishable, and (iv) the interchange of particles at interfaces between G_1 and G_2 takes place in such a manner as to preserve the number of particles in each subsystem. A fraction of frozen particles in the glass, χ, is defined which plays the role of the "configurational entropy" in their model. In practice, they assumed that the glass transition *may* be a second order phase transition, i.e., a compressibility jump, which has the practical advantage that only two unknown parameters enter Eq. (3). At a given value of η_g, the thermodynamic requirement of equal chemical potentials and pressures was utilized for phase coexistence. In the glass, particle centers are confined (by assumption) to finite regions of space of irregular shape but constant volume as schematically illustrated in Figure 2; note that the confined particles still interact with each another.

Like BV, we assume a second order fluid to glass transition which follows from equating the pressure and chemical potential at η_g and gives the first set of conditions

$$Z_{D,g}(\eta_g, p_1, p_2) = Z_{D,f}(\eta_g), \quad (4)$$

$$\mu_{D,g}(\eta_g, p_1, p_2) = \mu_{D,f}(\eta_g). \quad (5)$$

The hard sphere free energy per particle is[37,46]

$$\frac{F_{D,i}(\eta)}{Nk_BT} = \ln(\eta) + \int_0^\eta \left(\frac{Z_{D,i}(x) - 1}{x}\right) dx + C_{D,i}, \quad (6)$$

where the constants $C_{D,i}$ enter the low density excess free energy of phase i, and are necessary to distinguish between the low density fluid and the *hypothetical* low density glass in the cell model description. Such an approach is analogous to using a cell model for the fluid-to-crystal transition in hard spheres[46] where integration of the EOS to calculate chemical potentials results in a constant of integration. This technical cell model device is employed to *artificially* stabilize the glass phase down to the dilute limit to compute $C_{D,i}$ and the *absolute* entropy difference between two phases. If definite integration from a known entropy common reference point can be performed, then $C_{D,i}$ can be determined and phase coexistence found.

At first glance, the use of the dilute glass concept might seem in contradiction with the presence of a spinodal density limit below which the glass spontaneously melts. However, the confining cells at low density have no physical meaning beyond providing a path for thermodynamic integration up to relevant glass densities.[37,46] Other paths with more complex stabilization approaches could be constructed. At the relevant glass densities the particles are self-confined by repulsive force caging implying the cells contribute a negligible amount to the true free energy, thus yielding a useful estimate of the *true* unconfined glass free energy.[35,46] Now, in general, $C_{D,g} > C_{D,f}$ as the glass phase has a higher free energy. From Eq. (6) the chemical potential then follows as

$$\frac{\mu_{D,i}(\eta)}{k_BT} = \frac{F_{D,i}(\eta)}{Nk_BT} + Z_{D,i}(\eta). \quad (7)$$

We modify the BV work motivated by more modern views of the thermodynamic glass problem. Specifically, we adopt a spatially homogenous glass model composed of localized particles. For the D-dimensional fluid in the dilute limit the partition function is

$$Q_{D,f}(\eta \to 0) = \frac{V^N}{N!} \cong \left(\frac{eV}{N}\right)^N, \quad (8)$$

where V is the volume (or hyper volume for $D \geq 4$), N is the number of particles, e is Euler's number, and Stirling's approximation has been used. Very close to jamming, the particles only explore an effective volume, $V\eta_j$, where η_j is the jamming volume fraction. Individual particles are confined to regions of space (cells containing only 1 particle) of $\sim V\eta_j/N$, as schematically shown in Figure 2. The choice of cell volume is employed to allow the complexity, defined below, to be an approximate measure of the number of jammed configurations corresponding to the glass. Unlike BV, we assume that for a given glass there can be an enormous geometric degeneracy in dividing the total volume into N distinct cells in the sense that the number of configurations is extensive

$$\Omega \equiv \exp(N\Sigma), \quad (9)$$

where Σ is commonly called the complexity or configurational entropy associated with the number of cell configurations (basins) at fixed jamming packing fraction which we do not explicitly label with dimensionality. The fluid is viewed as being composed of an exponential number of relevant glass configurations found at η_g, or conversely, all of the combined cell model glass states compose the equilibrated fluid at η_g. Combining the above elements yields

$$Q_{D,g}(\eta \to 0) = \left(\frac{V\eta_j}{N}\right)^N \Omega. \quad (10)$$

Equation (10) would reduce to the BV low density form if $\eta_j \to 1$ and $\Omega \to 1$.

Using Eq. (8), the free energy of the dilute fluid is

$$\frac{F_{D,f}(0)}{Nk_BT} = \ln\left(\frac{N}{V}\right) - 1, \tag{11}$$

and for the hypothetical dilute glass using Eq. (10) one has

$$\frac{F_{D,g}(0)}{Nk_BT} = \ln\left(\frac{N}{V}\right) - \ln(\eta_j) - \Sigma. \tag{12}$$

Equations (6), (11), and (12) then yield

$$C_D \equiv C_{D,g} - C_{D,f} = 1 - \ln(\eta_j) - \Sigma. \tag{13}$$

One of the conditions determining p_1 and p_2, Eq. (5), can be restated using Eq. (13) with Eqs. (6) and (7) as

$$\int_0^{\eta_g}\left(\frac{Z_{D,f}(x)-1}{x}\right)dx = \int_0^{\eta_g}\left(\frac{Z_{D,g}(x,\,p_1,\,p_2)-1}{x}\right)dx + C_D. \tag{14}$$

One final constraint is required to determine the specific values of p_1, p_2, and Σ for a given η_g. Its derivation starts with the jamming point relation of Eq. (3)

$$\eta_j = \frac{2}{2^D - 2p_1 - 4}. \tag{15}$$

It is well known that the compressibility factor near jamming follows the seemingly exact free volume prediction[11,12,14]

$$\lim_{\eta\to\eta_j} Z_{D,g}(\eta) = \frac{D}{1-\eta/\eta_j}. \tag{16}$$

Combining Eq. (15) with Eqs. (3) and (16) produces the final condition uniquely determining p_1, p_2, and Σ for a specific η_g

$$1 + p_1\eta_j + p_2\eta_j^2 = D(1-\eta_j)^2. \tag{17}$$

By specifying η_g, and solving the coupled Eqs. (4), (14), and (17), very long and complicated analytical formulas for $p_1(\eta_g)$, $p_2(\eta_g)$, $\eta_j(\eta_g)$, and $\Sigma(\eta_g)$ are in principle obtainable. In the light of their highly unwieldy nature, we have opted to solve the coupled equations numerically, and hence we refrain from writing down the analytic formulas. In the high dimension limit (Sec. II C) the analytic solutions are much simpler and we present results for $\Sigma(\eta_g)$. Choosing a value for η_g is equivalent to choosing a specific complexity in RT, or simulation compression rate, corresponding to a particular glass. There is a one-to-one mapping between η_g and Σ, and hence multiple glasses. However, in both RT and our approach there is only one unique densest glass characterized by $\Sigma \to 0$. Using all of the results in this section the final compressibility factor is

$$Z_D(\eta) = \begin{cases} Z_{D,f}(\eta), & \eta < \eta_g \\ Z_{D,g}(\eta,\,p_1,\,p_2), & \eta_g \le \eta. \end{cases} \tag{18}$$

C. High dimension limit

Deriving the asymptotic limit for the equilibrium glass in high dimensions starts with Eq. (2) for the fluid and Eq. (3) for the glass. Taking the $D \to \infty$ limit of Eq. (2) yields

$$Z_{\infty,f}(\eta) \equiv \lim_{D\to\infty} Z_{D,f}(\eta) = 1 + 2^{D-1}\eta - 2^{D-1}A_D\eta^2. \tag{19}$$

As $D \to \infty$, we do not employ the fluid first virial correction form, $Z_{\infty,f}(\eta) \equiv 1 + 2^{D-1}\eta$,[15,18] since when using Eqs. (4), (14), and (17) and our glass EOS we find that no solution exists. Hence, including structural corrections via $-2^{D-1}A_D\eta^2$ is necessary as $D \to \infty$. Further analysis is simplified by adopting a scaled density, $\mathrm{H} \equiv 2^D\eta$, a scaled Carnahan-Starling parameter, $B_D \equiv 2^{-D}A_D$, and scaled coefficients for the glass EOS as $G_1 \equiv 2^{-D}p_1$, and $G_2 \equiv 2^{-2D}p_2$. Rewriting Eq. (19) using the scaled quantities one has

$$Z_{\infty,f}(\mathrm{H}) = \frac{1}{2}(2 + \mathrm{H} - \mathrm{H}^2B_D) \tag{20}$$

Taking the $D \to \infty$ limit of Eq. (3) for the glass EOS yields

$$Z_{\infty,g}(\eta) \equiv \lim_{D\to\infty} Z_{D,g}(\eta) = \frac{1 + p_1\eta + p_2\eta^2}{1 + (p_1 - 2^{D-1})\eta}, \tag{21}$$

or in terms of scaled quantities

$$Z_{\infty,g}(\mathrm{H}) = \frac{1 + G_1\mathrm{H} + G_2\mathrm{H}^2}{1 + (G_1 - 1/2)\mathrm{H}}. \tag{22}$$

From Eq. (22) the scaled jamming packing fraction is

$$\mathrm{H}_j = \frac{1}{1/2 - G_1}. \tag{23}$$

In the high dimension limit, one of the conditions determining the unknown glass EOS parameters, Eq. (4), can be rewritten using Eqs. (20) and (22)

$$Z_{\infty,g}(\mathrm{H}_g,\,G_1,\,G_2) = Z_{\infty,f}(\mathrm{H}_g). \tag{24}$$

The other condition, Eq. (17), can be easily restated in the $D \to \infty$ limit as

$$1 + G_1\mathrm{H}_j + G_2\mathrm{H}_j^2 = D, \tag{25}$$

where Eq. (23) can be inserted for H_j. Equations (24) and (25) can be solved analytically for $G_1(\mathrm{H}_g, B_D, D)$, and $G_2(\mathrm{H}_g, B_D, D)$, which when combined with Eq. (14), the various scaled quantities, and the high dimension equations of state of Eqs. (20) and (22), yield the high D complexity as

$$\begin{aligned}\Sigma(\mathrm{H}_g) = 1 - \ln\left[\frac{2^{2-D}D}{B_D\mathrm{H}_g + \sqrt{B_D\left(-8D + B_D\mathrm{H}_g^2\right)}}\right] \\ + D\Big(\ln[4] - \ln\Big[4 - D^{-1}\mathrm{H}_g\big(B_D\mathrm{H}_g \\ + \sqrt{B_D\big(-8D + B_D\mathrm{H}_g^2\big)}\big)\Big]\Big) \\ - \frac{1}{4}\mathrm{H}_g\sqrt{B_D\left(-8D + B_D\mathrm{H}_g^2\right)}.\end{aligned} \tag{26}$$

Calculation of the Kauzmann glass transition value of $\mathrm{H}_K \equiv 2^D\eta_K$ corresponds to determining the glass transition volume fraction where the complexity vanishes, $\Sigma(\mathrm{H}_K) = 0$. We find that numerical solution of Eq. (26) strongly suggests

$$B_D\mathrm{H}_K^2 = QD, \tag{27}$$

where Q is a D independent constant. Equation (27) is exact as $D \to \infty$. To prove this, we require the high D form of the CS A_D parameter and correspondingly B_D, which have been derived from Ref. 47. One then finds

$$\lim_{D\to\infty} B_D = -\frac{1}{2}\left(\frac{b_3}{b_2^2}\right) = -\left(\frac{6}{\pi}\right)^{1/2}\left(\frac{3^{1/2}}{2}\right)^D D^{-1/2}, \tag{28}$$

where b_2 and b_3 are the second and third D-dimensional hard sphere virial coefficients, respectively. Substituting Eqs. (27) and (28) into Eq. (26), and expanding the right-hand side of the equation in D about zero, gives

$$\Sigma(\mathrm{H}_K) = O(\ln(D)) + \frac{1}{4}(-\sqrt{Q(Q-8)} + \ln(3072) - 4\ln[4 - \sqrt{Q(Q-8)} - Q])D, \tag{29}$$

where $O(\ln(D))$ indicates a contribution of order ln (D). Since the first term grows slowly with dimension relative to the second term, solving $\Sigma(\mathrm{H}_K) = 0$ becomes through leading order equivalent to solving

$$\frac{1}{4}(-\sqrt{Q(Q-8)} + \ln[3072] - 4\ln[4 - \sqrt{Q(Q-8)} - Q]) = 0. \tag{30}$$

This equation for Q is independent of D, thereby proving that Q is a constant and Eq. (27) is exact as $D \to \infty$. Solving Eq. (30) numerically gives $Q \cong -5.3588527\ldots$.

The final high dimension form for $\mathrm{H}_K \equiv 2^D\eta_K$ then follows by combining Eq. (27) with Eq. (28) to obtain

$$\eta_K = \sqrt{-2QD}\left(\frac{b_2^2}{b_3}\right)^{1/2} 2^{-D}. \tag{31}$$

This result provides a possible link between the Kauzmann transition and the thermodynamic properties of hard sphere fluid based on the second and third virial coefficients. Using the high dimensional form of b_2 and b_3 in Eq. (31) yields

$$\eta_K = \frac{\pi^{1/4}\sqrt{-Q}2^{-\ln[6]/\ln[16]}D^{3/4}}{2^{(\ln[12]/\ln[16])D}} \cong \frac{1.96918\ldots D^{3/4}}{2^{0.896241\ldots D}}. \tag{32}$$

Analogously, a similar analysis of Eq. (23) for $\mathrm{H}_{GCP} \equiv 2^D\eta_{GCP}$ gives

$$\eta_{GCP} = \frac{kD^{3/4}}{2^{(\ln[12]/\ln[16])D}} \cong \frac{2.53914\ldots D^{3/4}}{2^{0.896241\ldots D}}, \qquad k \equiv 2^{\left(\ln\left[\frac{128\pi}{3}\right]+4\ln\left[\frac{1}{\sqrt{8-Q}-\sqrt{-Q}}\right]\right)/\ln[16]} \tag{33}$$

From Eqs. (32) and (33) we find that $\eta_{GCP} \cong 1.29\eta_K$, thereby suggesting the two important volume fractions are proportional in high dimension.

An interesting aspect of our work is that the dependences of the characteristic packing fractions on (high) spatial dimension differ qualitatively from recent MCT and RT predictions, as discussed in detail below. Whether this is correct is not known. As a caveat we note that our results follow from using a second order structural correction. This might reflect the fact that Eq. (3) is a not very good representation of the glass in the dilute limit at high D, even if it is accurate in lower dimensions. Interestingly, it is conjectured that as long as $2^D\eta$ is sub-exponential the first virial correction form is sufficient,[15,48] but we show below that in our theory the relevant volume fractions grow exponentially in large dimension consistent with requiring contact value corrections to the fluid EOS. Future work should attempt to include the exact low packing fraction behavior in our approach using cell model cluster expansion ideas.[46]

D. Summary of theoretical method

To further clarify our approach, this section summarizes the developments of Secs. II A–II C. As input, the theory adopts an accurate fluid EOS, typically some approximate virial series summation expression[11,12,15,27–31] (i.e., Eqs. (1) and (2)). For the glass EOS we use a scaled particle theory form[37] with two parameters, p_1 and p_2, which is believed to be reasonable for all amorphous states. The glass and fluid equations of state meet at a well-defined packing fraction, η_g, where a discontinuity or cusp is present in the compressibility or pressure, respectively. The parameters p_1 and p_2 are determined by enforcing continuity of pressure at η_g, and a divergence of the glass EOS at a jamming packing fraction, $\eta_j = 2/(2^D - 2p_1 - 4)$, that follows the free volume form $Z_{D,g}(\eta \to \eta_j) = D/(1 - \eta/\eta_j)$.

We then determine the configurational entropy or complexity by enforcing continuity of the chemical potential at η_g. A chemical potential difference, C_D, between the glass and fluid necessarily arises as an integration constant[37,46] which we evaluate via thermodynamic integration from an analytically known reference point.[37,46] The latter is chosen in direct analogy with the classic analysis of the hard disk and hard sphere crystallization transition by Hoover and Ree.[46] Of course, in reality diluting a glass state indefinitely is not possible due to a likely thermodynamic or mechanical instability.[15] Hence, the glass is *artificially* stabilized down to the dilute limit via hypothetical confining cells[37,46] characterized by two entropic components: (1) vibrations within the confining cells, and (2) a large geometric degeneracy in forming the cells leading to a nonzero complexity Σ. We emphasize that our definition of a "glass" in this framework contains both the configurational and vibrational contributions. The cells contain one particle in a volume $V\eta_j/N$ and the number of ways to partition space in this manner is Ω. Separation of these entropic contributions yields $C_D \equiv 1 - \ln(\eta_j) - \Sigma$, where $\Sigma \equiv N^{-1}\ln\Omega$ is the complexity. Enforcing equal glass and fluid chemical potentials at η_g then uniquely specifies Σ. The Kauzmann transition packing fraction then follows from the zero complexity condition, $\Sigma(\eta_g = \eta_K) \equiv 0$.

III. PREDICTIONS IN THREE DIMENSIONS

A. Background

Using the theory of Sec. II, multiple glass equations of state can be calculated for various choices of η_g. Arguably, η_g can be interpreted as the approximate location where the pressure departs from an accurate fluid virial series summation EOS. Simulation studies typically cite η_g as near the

empirically determined ideal MCT transition at $\eta_d \sim 0.57-0.58$.[10–12,18] MCT, DFT, and RT all view the crossover at η_d as arising from the partitioning of phase space into many deep disconnected free energy minima.[15–22]

Identifying characteristic packing fractions suggestive of a thermodynamic transition or crossover using simulation is subtle. Hermes and Dijkstra[11] found strong evidence for a thermodynamic signature of a glass transition at $\eta \sim 0.58$ based on a discontinuity in the *derivative* of the compressibility. We could extend Eq. (3) using another exact SPT criterion to include three fit parameters and enforce compressibility continuity (see the Appendix). However, the resulting equations are difficult to solve so the simpler two parameter form in Eq. (3) is adopted, and we believe the consequences of a compressibility jump for questions of present interest is minor.

Berthier and Odriozola (BO) recently used replica exchange (RE) Monte Carlo to simulate a 50/50 binary mixture of hard spheres with diameter ratio 1.4.[23] Convincing evidence was presented that thermal equilibrium is achieved up to $\eta \sim 0.62$. They find that at $\eta \sim 0.59$ the two component CS EOS[23,49] breaks down, and after a narrow crossover window free volume pressure growth sets in corresponding to

$$Z_{RE}(\eta) = \frac{2.82}{1-\eta/0.669}. \tag{34}$$

Free volume like behavior is a characteristic of a glass, not the traditional fluid described by re-summed virial expansions.[11,12,15,27–31] Near the crossover it was found that Monte Carlo thermalization suddenly became more difficult. Higher pressure replicas were ergodic only if the lowest coupled replica efficiently sampled $\eta \lesssim 0.58$. This simulation data[23] is shown in Figure 1. Of course it is possible that the observed "equilibrium" glass is not truly equilibrated but rather, due to practical simulation time constraints, aging is not perceived. Therefore, the possibility for an underlying thermodynamic phase transition at higher densities is not ruled out.

Santos *et al*. developed a theory[50] to infer the metastable EOS for monodisperse hard spheres from the BO simulation data[23] (see Fig. 1). The high density compressibility factor was predicted to be

$$Z_{HS}(\eta) = \frac{3}{1-\eta/0.668}, \tag{35}$$

which is very similar to the binary mixture simulation results.[23] Additional non-trivial predictions[50] suggest that their theory accurately represents metastable monodisperse hard spheres which can jam into an amorphous state at packing fractions greater than ~0.64.

B. Theory calculations

We now present calculations in 3-dimensions based on our approach. Four representative glass continuations of the fluid EOS are shown in Figure 1 with chosen $\eta_g = 0.5$, 0.545, 0.581, and 0.611, leading to *predicted* jamming packing fractions of $\eta_j = 0.630$, 0.650, 0.668, and 0.684, respectively. The complexities associated with the four glass branches are $\Sigma(\eta_g) = 1.035$, 0.743, 0.404, and 0, respectively, where the vanishing complexity is associated with the equilibrium glass.

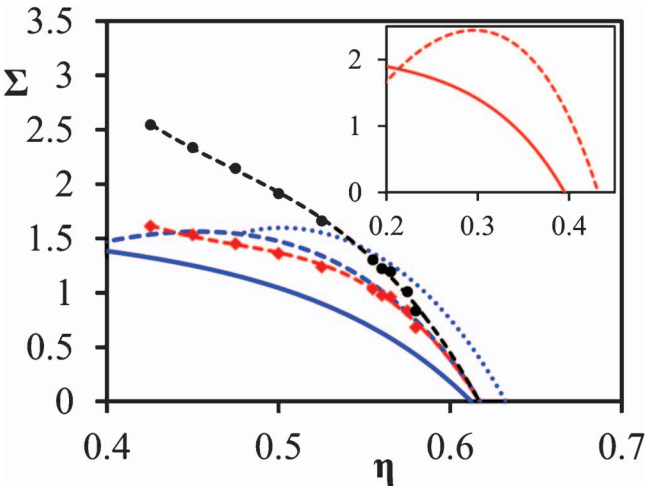

FIG. 3. Dimensionless complexity per particle as a function of (chosen glass transition) packing fraction demonstrating the vanishing of the complexity at η_K corresponding to the densest (equilibrium) glass that jams at η_{GCP}. Dashed and solid blue curves indicate the replica theory results[15] and our calculations, respectively; the dashed and solid red curves in the inset are the analogous 4D calculations. For the 3D case the approach of Stillinger *et al*.[51] is represented by the dotted blue line which subtracts the crystal entropy from the fluid entropy at equal pressure. Red diamonds and black circles are simulation data of Angelani and Foffi[34] determined in two slightly different ways; the dashed curves through the points are third order polynomial fits shown for visual aid only. Within the replica approach, $\eta_K = 0.618$ and $\eta_{GCP} = 0.684$ in 3D, and $\eta_K = 0.432$ and $\eta_{GCP} = 0.487$ in 4D (inset). The analogous 3D results within our theory are $\eta_K = 0.612$ and $\eta_{GCP} = 0.684$, and $\eta_K = 0.395$ and $\eta_{GCP} = 0.462$ in 4D (inset). The simulation calculations of Angelani and Foffi[34] extrapolate to $\eta_K \cong 0.62$ and the theory of Stillinger *et al*.[51] leads to $\eta_K \cong 0.632$.

Figure 3 shows examples of the complexity as a function of packing fraction for 3D (and also 4D) hard spheres. When $\Sigma \to 0$ at η_K, the system becomes stuck in the densest glass state and further compression ultimately leads to jamming at η_{GCP}. Intuitively, one expects Σ increases with spatial dimension, as found in Figure 3 for calculations in 3D and 4D. We show in Sec. IV A that the equilibrium glass of our theory appears to be representative of the densest glass that can be obtained by ultra-slow simulation compressions and departs from the fluid EOS at $\eta_g(0) \equiv \eta_g(\Gamma \to 0)$, and then jams at $\eta_j(0) \equiv \eta_j(\Gamma \to 0)$ in $D = 3$–12 (using a power law extrapolation). In our theory, slower compression rate corresponds to smaller complexities, Σ, and hence we write $\eta_K \equiv \eta_g(\Sigma \to 0)$ and $\eta_{GCP} \equiv \eta_j(\Sigma \to 0)$. As discussed both below and in depth in Sec. IV A, the equivalence of the $\Sigma \to 0$ glass predicted by our theory and that extracted from simulation is only a working hypothesis which is definitely arguable given uncertainties in the precise physical meaning of simulation extracted characteristic packing fractions.

Figure 1 also presents a specific comparison with the simulation data for monodisperse hard spheres of Speedy[24] and the polydisperse data of Hermes and Dijkstra.[11] Comparison of polydisperse (or mixture) hard sphere data with monodisperse data must be done carefully since polydispersity increases the jamming density,[11,16] speeds up dynamics,[42,43] and lowers the pressure.[42,43] However, the moderate 10% polydispersity case,[11] which we compare to Figure 1, possesses a fluid EOS nearly identical to the monodisperse case. We assume the matching fluid regime implies a similar glassy

regime. This is reasonable given that at *any fixed* compression rate the 10% polydispersity jamming point, $\eta_{j,10\%}(\Gamma)$, is only slightly augmented over the monodisperse jamming point, $\eta_{j,mono}(\Gamma)$, by $\eta_{j,10\%}(\Gamma) - \eta_{j,mono}(\Gamma) \cong 0.003$.[11] We find that the combined monodisperse and polydisperse simulation data departs the CS EOS at $\eta_g \cong 0.545$. Using this value in our calculations, the theory describes the simulation data well, and $\eta_j = 0.650$ and $\Sigma(\eta_g) = 0.743$ is predicted; this Σ value suggests the system is not fully aged or equilibrated (not densest branch). More interestingly, the densest "equilibrium" glass corresponding to $\Sigma(\eta_K) = 0$ is predicted to occur at $\eta_K = 0.612$, and jam at $\eta_{GCP} = 0.684$. The latter is close to the *monodisperse* predictions of Santos *et al.*[50] at $\eta_{GCP} = 0.668$. Our predicted densest glass is more concentrated than the latter result, though, interestingly, it is close to the small cage replica ideal glass jammed state at $\eta_{GCP} \sim 0.684$.[15] If we choose $\eta_g = 0.581$, then our theory predicts $\eta_j = 0.668$ and a smaller complexity $\Sigma(\eta_g) = 0.404$. The entire EOS shown in Figure 1 agrees well with the Santos *et al.* theory[50] except right near the glass transition; this choice of glass branch will be used in Paper II[55] since it has some simulation/theory based validation[23,50] and the structural predictions of Paper II[55] vary little with the choice of glass branch.

The similarity in 3D of our predicted η_K and η_{GCP} for the densest glass with that of the replica theory makes it tempting to assume our theory corresponds to the *ideal* glass picture of replica theory. However, the ideal glass is not necessarily the same as the "equilibrium" glass deduced in compression simulations since the extrapolations employed to determine $\eta_g(0)$ and $\eta_j(0)$ are sensitive to both spatial dimensionality and the assumed extrapolation functional form (discussed at the end of Sec. I C). Recall it is possible that $\eta_g(0)$ and $\eta_j(0)$ are closer to η_d and η_{th} rather than η_K and η_{GCP}, respectively. Some insight concerning this issue is obtained in the next section, Sec. IV, where we compare our results with simulations and RT calculations up to 12 dimensions.

Figure 3 also shows that the functional form of the complexity within the replica theory,[15] the Stillinger *et al.* approach,[51] the simulation deduced results of Angelani and Foffi,[34] and our theory, are not too different in $3D$. Moreover, the zero complexity state occurs at essentially the same packing fraction, which is especially interesting given all the approaches employ different measures of Σ. We do note that the simulation data of Angelani and Foffi[34] utilized a binary mixture with diameter ratio 1.2; however, this particular mixture differs little from the monodisperse case for both thermodynamic[34] and jamming properties.[16] Both RT[15] and the simulation approach[34] counts stable amorphous minima in the fluid directly, while the Stillinger approach[51] subtracts the 3D HS crystal entropy from the fluid at equal pressure to roughly count configurations, and our theory roughly counts limiting jammed configurations. Transitioning from 3D to 4D increases the overall magnitude of Σ, in both RT and our approach, as expected. Within the replica calculations, Σ is nonmonotonic and goes through a maximum, a feature possibly related to limitations of the small cage expansion. Additionally, we find (not shown) that if we plot the complexity from the replica approach or our theory versus the dimensionless inverse compressibility, $S_0^{-1} \equiv S^{-1}(q = 0)$, or the compressibility factor, Z, a linear relationship is found in the low complexity regime.

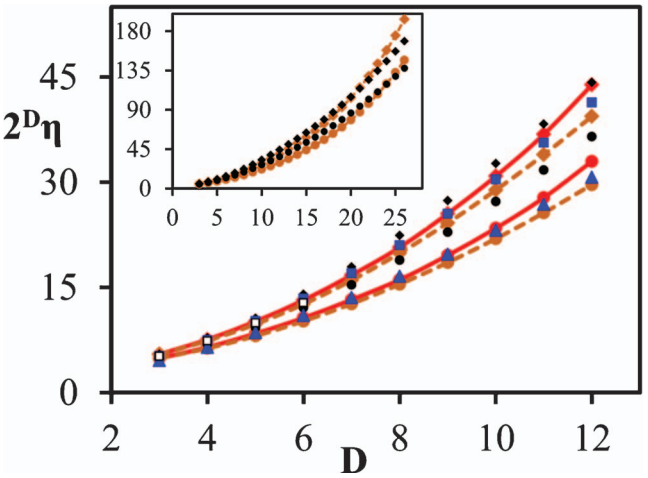

FIG. 4. Our SPT theory predictions for hard spheres in 3 to 12 dimensions for η_K (solid curve with red spheres) and η_{GCP} (solid curve with red diamonds) (multiplied by 2^D) using the simulation adjusted CS fluid EOS of Charbonneau *et al.*[18] Dashed curves with orange circles and triangles are analogous calculations using the traditional CS formula.[27,28] Interpolation curves are a visual aid. These theoretical results are compared to simulation extrapolated values[18] for $\eta_g(0)$ (small blue triangles) and $\eta_j(0)$ (small blue squares). Replica predictions[15,18] for η_K (small black circles) and η_{GCP} (small black diamonds) are also shown. MRJ results[12] from compression simulations are shown as white squares from $3 \le D \le 6$. (Inset) Same as main frame (without simulation adjusted CS form) but extended to higher dimension.

IV. RESULTS IN HIGH DIMENSIONS

A. Three to twelve dimensions and comparison to simulation

Figure 4 compares our predicted densest glass η_K and η_{GCP} in 3 to 12 dimensions to the $\eta_g(0)$ and $\eta_j(0)$ simulation data of Charbonneau *et al.*[18] obtained using a power law extrapolation. Surprisingly good agreement is found, except for the highest dimensionalities. What might be the significance of this level of quantitative agreement? We can think of at least two different possibilities. (i) The free energy barriers separating metastable glassy states grow slow enough with increasing D over the probed range that our "densest glass" calculations are plausibly probed in the simulation. If true, then the agreement is theoretically significant. The discrepancy at higher D would then suggest a breakdown of our theory as barriers become sufficiently large. (ii) Alternatively, the barriers grow very rapidly with increasing dimension even in the range of D = 3–12, and the lower dimensional agreement between theory and simulation is largely a fortuitous cancellation of errors. Under this scenario, our theory for η_K and η_{GCP} can be interpreted as providing increasingly distant upper bounds to both $\eta_g(0)$ and $\eta_j(0)$, respectively.

Although a truly definitive conclusion cannot be drawn, the second scenario is plausible since increased dimensionality presumably promotes higher barriers separating metastable states.[15,18] At a minimum, quantitative knowledge of the latter is necessary to make more definitive statements. Paper II[55] discusses the 3D nonlinear Langevin equation

(NLE) theory[25] which can approximately compute dynamical barrier heights albeit at the highly simplified single particle level. However, NLE theory requires nontrivial development to treat higher dimensions, including reliable higher dimensional structural input. These theoretical elements are presently not available, and work in this direction is beyond the scope of this article.

If the first scenario stated above applies, then the surprisingly good quantitative agreement of our theory with Charbonneau *et al.*[18] tempts us to identify our computed densest glass as best corresponding to the densest glass deduced from simulation extrapolations in $D \cong 3$–10 (using a power law form), and not the replica theory ideal glass that is usually viewed as inaccessible and possibly distinct from the practical simulation extrapolated glass. Our cell model based theory lends insight to what physics may lead to the simulation extrapolated densest glass as elaborated on in Secs. V and VI.

The replica theory η_K and η_{GCP} predictions are also shown in Figure 4. It is clear that $\eta_{GCP} \sim \eta_j(0)$, however $\eta_K > \eta_g(0)$. Two distinct interpretations seem possible. The first is that $\eta_g(0)$ and $\eta_j(0)$ should coincide with the replica predictions for η_K and η_{GCP}. However, the $\eta_g(0) = \eta_K$ equality may be masked by quantitative errors in the replica theory calculations based on the Gaussian small cage expansion.[15] To validate this conclusion will require work on two fronts: (i) systematic improvement of the small cage expansion, and (ii) simulation evaluation of the complexity in $D = 4$–12 for direct determination of η_K as done by Angelani and Foffi in 3D.[34] A second possible interpretation is that replica theory is correct in the sense that $\eta_K > \eta_g(0)$ and $\eta_{GCP} > \eta_j(0)$, and there is a reasonably well-defined densest glass found in simulation and a *different*, essentially impossible to explore via simulation, ideal glass at even higher densities. The simulation densest glass may be controlled by a numerical bottleneck related to the large times necessary to explore activated processes.[18] This scenario perhaps suggests that the replica theory measure of complexity differs from ours which seemingly terminates near the simulation densest glass in $D \cong 3$–10, and not the RT ideal glass. Again, definitive evaluation of this scenario will require replica small cage expansion improvements as well as further simulations that directly measure the complexity. Significant improvements are also likely needed for our simple SPT based approach. Tentatively, our interpretation is that the replica theory and our approach provide different bounds on the simulation extrapolated densest glass in $D = 3$–12.

B. High dimension regime

Sphere packings in dimensions far above three, while abstract, are of high recent interest in glass and jamming physics and also in the very different context[52] of error correcting codes. However, exact results do not exist for $D > 3$,[1,15,38–40] and the current state of the art relies on bounds for the maximal density. The best known rigorous upper bound[39] on the maximum sphere packing fraction is

$$2^D \eta_{max} \leq 2^{0.4010...D}, \tag{36}$$

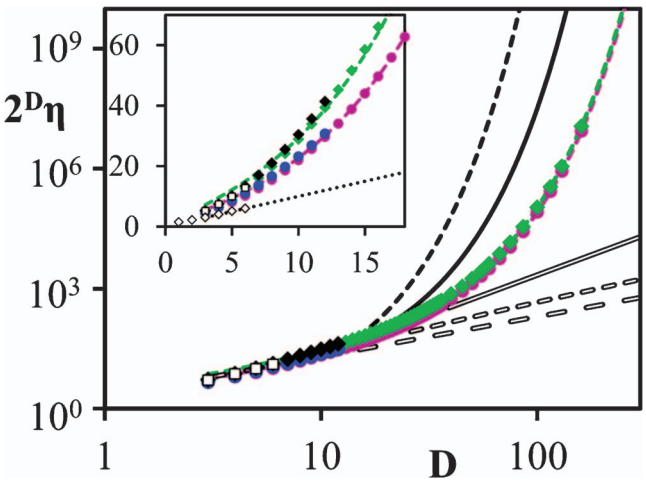

FIG. 5. Numerical SPT theory predictions for hard spheres in 3 to 205 dimensions for η_K (solid pink spheres) and η_{GCP} (solid green diamonds) (multiplied by 2^D) using the CS fluid EOS[27,28] presented in log-log format. Solid blue circles and solid black diamonds from $3D \rightarrow 12D$ are the analogous simulation results for $\eta_g(0)$ and $\eta_j(0)$, respectively.[18] Dashed pink and green lines are the theoretical high D scaling forms for η_K and η_{GCP}, respectively. The solid dashed black curve represents the best known upper bound on the maximum achievable packing in high dimensions.[39] The solid black curve is the conjectured best lower bound on the maximum achievable packing and corresponds to amorphous jammed structures.[40] The open solid, small dashed, and large dashed curves are the high D MCT,[18,22] replica theory,[15,18] and Ball lower bound[38] predictions, respectively. Open squares are the MRJ compression simulation values.[12] (Inset) Expanded view showing the breakdown of the high D scaling form below $D \sim 10$. Open diamonds are RSA simulation saturation volume fractions[53] and the dotted line the apparent high D RSA scaling.

and is shown in Figure 5. Analogously, the best rigorous lower bound due to Ball[38] is

$$2^D \eta_{max} \geq 2D \tag{37}$$

and is also shown in Fig. 5. Interestingly, Torquato and Stillinger[40] have developed an exponential improvement on Eq. (37) based on a conjecture about amorphous packings in high dimension given by

$$2^D \eta_{max} \geq \frac{D^{1/6} 2^D}{2^{2/3} W \sqrt{\pi} 2^{(3-\log_2[e])\frac{D}{2}}} \cong 3.276101...D^{1/6} 2^{0.22135...D}, \tag{38}$$

where $W \cong 0.108488....$ This form is also shown in Figure 5. Equation (38) surpasses the densest known periodic arrangements for $D > 56$ suggesting in high dimensions certain classes of amorphous states may be thermodynamically stable relative to crystals at very high density.

Our predictions for the characteristic packing fractions in high dimensions, derived in Sec. II C, scale as $2^D \eta_{GCP} \sim 2^{fD}$, where $f > 0$. Specifically, the equilibrium glass and jamming packing fractions are

$$2^D \eta_K \cong 1.96918...D^{3/4} 2^{0.103759...D}, \tag{39}$$

$$2^D \eta_{GCP} \cong 2.53914...D^{3/4} 2^{0.103759...D}. \tag{40}$$

These analytic formulas are plotted in Figure 5, and pass essentially exactly through our numerically determined theoretical values of η_K and η_{GCP}. Rather remarkably, the high

D scaling forms works well down to $D \sim 10$. Significantly, we predict the thermodynamic glass transition and jamming packing fractions grow much more strongly than either RT[15,18] or MCT[18,22] which obey, respectively,

$$2^D \eta_K, \quad 2^D \eta_{GCP} \sim D \ln(D), \tag{41}$$

$$2^D \eta_{MCT} = 0.22 D^2. \tag{42}$$

Though RT and MCT differ in the "prefactor" dependence on spatial dimension, they both predict the characteristic packing fractions decrease in a simple exponential manner with dimension, i.e., $\propto 2^{-D}$, in contrast to Eqs. (39) and (40). Neglecting numerical pre-factors, the scaling laws of Eqs. (41) and (42) are plotted in Figure 5.

Unfortunately, no definitive conclusion can be made at this point regarding whether our high dimensional predictions are correct. However, we can offer speculative arguments for why our theory might be correct. If amorphous packings are the densest states in high dimensions, then ultra-slow quasi-equilibrium compression of a fluid would intuitively lead to densities that scale in a similar fashion as the maximal jamming density especially if amorphous packings are maximally dense. This suggests compressing a fluid would lead to terminal jamming densities that grow as $2^D \eta_j \sim 2^{fD}$ where $f > 0$, as we predict. Although the RT and MCT results grow much more slowly in large dimensions than our theory, our calculations seem to agree a little bit better with numerical data for $3 \leq D \leq 12$ as shown in Figure 4. The reason for the agreement is not understood though, and of course it could be fortuitous. Growing discrepancies between our theory and the simulation results at the highest dimensionalities may be the first sign of our very strong exponential growth in η_K and η_{GCP} as per Eqs. (39) and (40). As already mentioned, our theory and RT predictions seemingly provide different bounds to $\eta_g(0)$ and $\eta_j(0)$, however our bounds may be worse in very high dimensions.

Torquato and co-workers[40,53] have demonstrated that a packing class generated via the so-called random sequential addition procedure (RSA) apparently scales as $2^D \eta_j \sim D$ at high D. The saturation densities achieved from RSA are very limited as demonstrated in the inset of Figure 5. Can an improvement by a weak factor of $\ln(D)$, according to replica theory,[15] then lead to the scaling of the jamming densities found from ultra-slow compressions of the hard sphere fluid? Only future simulations extended to extremely high dimensions will answer this question. However, we do note that the replica approach has been verified in mean field models to give the correct result.[15] This is an argument for the reliability of the scaling in Eq. (41) since high dimensionality presumably promotes mean field behavior in the sense of diverging barriers separating metastable states. Our theory also disagrees with the MCT scaling[22] in high dimension, although for the opposite reason as in RT since replica ideas suggest the high dimensional MCT scaling of Eq. (42) is too strong, while our approach suggests it is too weak. Of course, as mentioned at the end of Sec. II C, the stability of our present conclusions to improving the theory at low packing fractions possibly relevant to high D remains to be further investigated.

V. COMPARISON WITH REPLICA THEORY

Overall, our viewpoint has similarities and differences with the replica approach. Comparisons with RT, DFT, and MCT have been partially discussed in the context of specific issues in Secs. III and IV. Here, we attempt to briefly summarize these differences in a more qualitative, conceptual manner.

Replica theory predicts the emergence of a finite complexity and amorphous states (glasses) at η_d. With increasing densification (at equilibrium), a Kauzmann transition[15] at η_K is predicted where the replica complexity per particle vanishes, $\Sigma_R \to 0$. The latter is proportional to the logarithm of the number of free energy basins, $\Omega_R(f)$, at a given free energy, f, in phase space[15]

$$\Sigma_R(f) \equiv N^{-1} \log \Omega_R(f). \tag{43}$$

The f of a basin (by definition) can be calculated by restricting the partition function to configurations in phase space that, upon a compression, would lead to the same jammed configuration at η_j.[15] In between η_d and η_K, multiple glass branches can be followed by probing a particular glassy basin complexity,[15] and if thermal equilibrium is maintained the normal fluid EOS (i.e., virial series summation) holds up to η_K. Following different glass branches is viewed as corresponding to different compression rates in simulations, and RT motivated physical arguments suggest that exploring glassy branches past η_d may require exponentially slow compaction rates, $\Gamma < \exp(-\#D)$,[18] a possible physical interpretation as to why the VFT based $\Gamma \to 0$ extrapolation may tend to η_K in simulation. Beyond η_K, free volume pressure growth occurs on the ideal glass branch which terminates with a divergent pressure at η_{GCP}.

One possible interpretation of our analysis is that the simulation deduced $\eta_g(0)$ and $\eta_j(0)$ roughly correspond to the zero complexity η_K and η_{GCP} of our theory. We propose that near $\eta_g(0)$ the number of ways to assign each particle a volume $V\eta_j/N$ becomes sub-extensive. Densification past $\eta_g(0)$ is difficult and requires finding jammed states with less total accessible volume (combined cell volume) than the total volume the particles physically occupy, perhaps related to the onset of non-trivial free energy barriers. In a sense, the simulation realizable (practical) glassy EOS continuations vanish, reminiscent of a Kauzmann transition, and beyond this density there is no longer an "effective fluid" region of configuration space. From a practical point of view, our theory provides a possible upper bound to what is attainable from simulation measurements due to growing numerical expense associated with larger barriers. As a caveat, we note that there is some ambiguity in the concept of complexity, which is tied to the particular glass model and theory used. We also emphasize that the RT analog of η_d is not predicted by our simple approach, and the irregular cell model as a description of metastable glass states is adopted by ansatz.

Overall, we view the equilibrium glass as the practical continuation of the fluid EOS that incorporates jamming and the physics missing in re-summed fluid virial expansions, in the spirit of the idea that fluid-based virial expansions cannot thermodynamically describe crystals.[11,12,15,27–31] We

suggest there is a densest glass that continues the fluid with a pressure higher than predicted by normal liquid equations of state. Below $\eta_g(0)$, we view the fluid as composed of an extensive number of *hypothetical* or *potential* metastable glassy states corresponding structurally to the equilibrated fluid at a given η. Such states can be probed by restricting the partition function using the amorphous cell model.[37,46] On the computer or in the laboratory, this is realized by rapid enough compression which traps the configuration until the pressure diverges.[10–12,18] We expect the glassy EOS branches deduced from our theory to become increasingly accurate closer to the equilibrium glass, i.e., the denser, stronger confined metastable states with weaker aging effects.

VI. SUMMARY AND DISCUSSION

We have developed a new, rather simple, equilibrium theory for the thermodynamics of glassy phases of monodisperse hard spheres that allows the calculation of the EOS and glass transition and jamming packing fractions for spatial dimensions of three and higher. A well-defined densest glass continuation of the fluid EOS is predicted which we refer to as the equilibrium glass (also called the ideal glass). In 3-dimensions, we find the densest glass to originate from a Kauzmann transition at $\eta_K = 0.612$, followed by jamming at $\eta_{GCP} = 0.684$, in reasonable agreement with recent simulations[10,18,23] and another theory.[51] Up to 12 dimensions the agreement between our theory and simulation equilibrium glass packing fractions is surprisingly good. However, the theoretical significance of this level of agreement remains unclear, for both conceptual and practical computational reasons, and it could be fortuitous. More research is required for crisper conclusions to be drawn.

If the agreement of the simulation determined $\eta_g(0)$ values with our theoretically computed ones is not an accident, then it suggests the former is measuring a quantity at least tightly correlated with a vanishing complexity, Σ. In our theory, the latter is the number of geometrically distinct ways to arrange particle centers confined in irregular cells, and is a rough measure of the number of jammed configurations. Beyond $\eta_g(0)$ any EOS found from even the most refined virial series summations is postulated to be unrealizable either rigorously or just due to the practical limitations of the enormous equilibration times associated with the predicted jammed packing bottleneck in configuration space. Our theory shares significant similarities with the replica approach,[15] but there are also differences conceptually, numerically, and with regards to scaling laws with spatial dimension for the characteristic packing fractions. Resolving these differences requires future theoretical and simulation research. It is also desirable to extend our approach to multi-component systems given the large simulation literature on hard sphere mixtures. Paper II[55] builds on the developments in this paper to construct a thermodynamically self-consistent integral equation theory of the pair structure of equilibrium 3D monodisperse hard spheres, and utilizes it to study single particle activated hopping dynamics.

ACKNOWLEDGMENTS

We acknowledge informative and stimulating discussions and correspondence with Sal Torquato. We thank Michiel Hermes and Marjolein Dijkstra for sending us their polydisperse hard sphere data, and Gerardo Odriozola and Ludovic Berthier for sending us their binary mixture data. Finally, we thank both reviewers of the article for their constructive and valuable criticisms and suggestions. This work was supported by DOE-BES under Grant No. DE-FG02-07ER46471 administered through the Seitz Materials Research Laboratory.

APPENDIX: DERIVATION OF THE SCALED PARTICLE THEORY GLASS EQUATION OF STATE

SPT focuses on the conditional pair nearest neighbor distribution function, $G(r;\eta)$, where $\rho G(r;\eta)$ is the density of particles in a spherical shell of radius r given that there are no other particles within this region except a tagged particle at the origin. In general, $G(r;\eta)$ is a complicated function, but at small separations follows exactly from geometry as[54]

$$G(r;\eta) = \frac{1}{1-2^D r^D \eta}, \quad 0 \le r \le 1/2. \tag{A1}$$

Here $G(r;\eta)$ satisfies a number of exact conditions, but only a few do not require correlation functions beyond the pair level. The first and simplest follows from Eq. (A1)

$$G(1/2;\eta) = \frac{1}{1-\eta}. \tag{A2}$$

Reiss *et al.*[54] proved that $G(r;\eta)$ is continuous across $r = 1/2$ at the first and second derivative level only. Taking the derivative of Eq. (A1) yields the second exact condition

$$G'(1/2;\eta) = \frac{2D\eta}{(1-\eta)^2}. \tag{A3}$$

The equality $G(1;\eta) = g(1)$ ($g(1)$ is the radial distribution function at contact) applies since at contact there can be no other particles in between and nearest neighbors are irrelevant, yielding

$$Z_D = 1 + 2^{D-1}\eta G(1;\eta). \tag{A4}$$

The final exact constraint we employ follows from realizing that as $r \to \infty$ the spherical void surface looks like a flat wall to the fluid particles, thus

$$G(\infty;\eta) = Z_D. \tag{A5}$$

The functional form for $G(r;\eta)$ is often written for $r > 1/2$ as a Laurent series which captures the exact $r \to \infty$ behavior as

$$G(r;\eta) = G(\infty;\eta) + \frac{A(\eta)}{r} + \frac{B(\eta)}{r^2} + \ldots. \tag{A6}$$

The coefficients $A(\eta)$ and $B(\eta)$ are typically determined by enforcing conditions like Eqs. (A2)–(A5), and perhaps others. While Eq. (A6) is known to be a good approximation, Baeyens and Verschelde[37] advocated using a more general series expansion truncated at three terms

$$G(r;\eta) = G(\infty;\eta) + A(\eta)t(r) + B(\eta)u(r) + \ldots, \tag{A7}$$

where $t(r)$ and $u(r)$ are linearly independent functions which allow the series to converge more rapidly than in Eq. (A6). For the hard sphere *fluid*, $t(r)$ and $u(r)$ were determined[37] by requiring the exact low density expansion of Eq. (A7) agrees with the exact low density expansion of $G(r;\eta)$. Here we are not interested in $t(r)$ and $u(r)$ in the *glass* but rather how they determine the EOS of Eq. (3) in the main text.

To proceed, one substitutes Eq. (A7) in Eq. (A2)

$$t_1 A(\eta) + u_1 B(\eta) + \frac{1}{2} Z_D(\eta) = \frac{1}{2(1-\eta)}, \tag{A8}$$

where $t_1 = t(1/2)/2$ and $u_1 = u(1/2)/2$. Similarly, using Eq. (A7) in Eq. (A3) yields

$$t_2 A(\eta) + u_2 B(\eta) = \frac{-D\eta}{2(1-\eta)^2}, \tag{A9}$$

where $t_2 = -t'(1/2)/4$ and $u_2 = -u'(1/2)/4$. Finally using Eqs. (A7), (A5), and (A4), one can derive a third equation (using $t(1) = 1$ and $u(1) = 1$)

$$2 + 2^D \eta (Z_D(\eta) + A(\eta) + B(\eta)) = 2 Z_D(\eta). \tag{A10}$$

Solving Eqs. (A8)–(A10) for $A(\eta)$, $B(\eta)$ and $Z_D(\eta)$ then yields

$$Z_D(\eta) = \frac{1 + p_1\eta + p_2\eta^2}{(1-\eta)^2(1 + (p_1 - (2^{D-1} - 2))\eta)}, \tag{A11}$$

$$p_1 = \frac{2^D t_2 - 8 t_2 u_1 - 2^D u_2 + 8 t_1 u_2}{4 t_2 u_1 - 4 t_1 u_2}, \tag{A12}$$

$$p_2 = \frac{2^D D t_1 - 2^D t_2 - 2^D D u_1 + 4 t_2 u_1 + 2^D u_2 - 4 t_1 u_2}{4 t_2 u_1 - 4 t_1 u_2}, \tag{A13}$$

which completes the derivation of Eq. (3).

In principle, further exact criterion on $G(r;\eta)$ could be used for better accuracy, and with each additional criterion another term in the expansion of Eq. (A7) is kept, thereby systematically improving the calculation of $Z_D(\eta)$. For example, with a third fitting parameter a continuous variation of the compressibility across the glass transition could be enforced. We have examined this route, but the resulting coupled equations are extremely unwieldy. Eventually >2 body correlations will enter in exact constraints on $G(r;\eta)$ fundamentally limiting the number of flexible parameters that can be included in a tractable manner.

[1] For recent reviews, see: S. Torquato and F. H. Stillinger, Rev. Mod. Phys **82**, 2633 (2010); A. J. Liu and S. R. Nagel, Annu. Rev. Condens. Matter Phys. **1**, 347 (2010).
[2] G. Brambilla, D. El Masri, M. Pierno, L. Berthier, L. Cipelletti, G. Petekidis, and A. B. Schofield, Phys. Rev. Lett. **102**, 085703 (2009).
[3] P. N. Pusey and W. van Megen, Phys. Rev. Lett. **59**, 2083 (1987); W. van Megen, T. C. Mortensen, S. R. Williams, and J. Müller, Phys. Rev. E **58**, 6073 (1998).
[4] G. L. Hunter and E. R. Weeks, Rep. Prog. Phys. **75**, 066501 (2012).
[5] Z. Cheng, J. Zhu, P. M. Chaikin, S. E. Phan, and W. B. Russel, Phys. Rev. E **65**, 041405 (2002).
[6] N. Xu, T. K. Haxton, A. J. Liu and S. R. Nagel, Phys. Rev. Lett. **103**, 245701 (2009); M. Schmiedeberg, T. K. Haxton, S. R. Nagel, and A. J. Liu, Europhys. Lett. **96**, 36010 (2011).
[7] P. E. Ramirez-Gonzalez, L. Lopez-Flores, H. Acuna-Campa, and M. Medina-Noyola, Phys. Rev. Lett. **107**, 155701 (2011).
[8] J.-P. Hansen and J. R. McDonald, *Theory of Simple Liquids*, 3rd ed. (Academic, New York, 2005).
[9] D. A. McQuarrie, *Statistical Mechanics* (University Science Books, Sausalito, CA, 2000).
[10] L. Berthier and T. A. Witten, Phys. Rev. E **80**, 021502 (2009).
[11] M. Hermes and M. Dijkstra, Europhys. Lett. **89**, 38005 (2010); J. Phys.: Condens. Matter **22**, 104114 (2010).
[12] M. Skoge, A. Donev, F. H. Stillinger, and S. Torquato, Phys. Rev. E **74**, 041127 (2006).
[13] S. Torquato, T. M. Truskett, and P. G. Debenedetti, Phys. Rev. Lett. **84**, 2064 (2000).
[14] R. D. Kamien and A. J. Liu, Phys. Rev. Lett. **99**, 155501 (2007).
[15] G. Parisi and F. Zamponi, Rev. Mod. Phys. **82**, 789 (2010); M. Mezard and G. Parisi, J. Chem. Phys. **111**, 1076 (1999); H. Yoshino, *ibid.* **136**, 214108 (2012).
[16] I. Biazzo, F. Caltagirone, G. Parisi, and F. Zamponi, Phys. Rev. Lett. **102**, 195701 (2009).
[17] H. Jacquin, L. Berthier, and F. Zamponi, Phys. Rev. Lett. **106**, 135702 (2011); L. Berthier, H. Jacquin and F. Zamponi, Phys. Rev. E **84**, 051103 (2011).
[18] P. Charbonneau, A. Ikeda, G. Parisi, and F. Zamponi, Phys. Rev. Lett. **107**, 185702 (2011); P. Charbonneau, E. I. Corwin, G. Parisi, and F. Zamponi, *ibid.* **109**, 205501 (2012); P. Charbonneau, A. Ikeda, G. Parisi, and F. Zamponi, Proc. Natl. Acad. Sci. U.S.A. **109**, 13939 (2012).
[19] P. Chaudhuri, L. Berthier, and S. Sastry, Phys. Rev. Lett. **104**, 165701 (2010).
[20] T. R. Kirkpatrick and P. G. Wolynes, Phys. Rev. A **35**, 3072 (1987); V. Lubchenko and P. G. Wolynes, Annu. Rev. Phys. Chem. **58**, 235 (2007).
[21] W. Götze and L. Sjogren, Rep. Prog. Phys. **55**, 241 (1992); W. Gotze, *Complex Dynamics of Glass Forming Liquids: A Mode Coupling Theory Approach* (Oxford University Press, Oxford, 2008).
[22] A. Ikeda and K. Miyazaki, Phys. Rev. Lett. **104**, 255704 (2010).
[23] G. Odriozola and L. Berthier, J. Chem. Phys. **134**, 054504 (2011).
[24] R. Speedy, J. Chem. Phys. **100**, 6684 (1994); J. Phys.: Condens. Matter **9**, 8591 (1997); **10**, 4387 (1998).
[25] K. S. Schweizer, J. Chem. Phys. **123**, 244501 (2005); K. S. Schweizer and E. J. Saltzman, *ibid.* **119**, 1181 (2003).
[26] K. S. Schweizer, Curr. Opin. Colloid Interface Sci. **12**, 297 (2007); E. J. Saltzman and K. S. Schweizer, Phys. Rev. E **77**, 051504 (2008).
[27] N. F. Carnahan and K. E. Starling, J. Chem. Phys. **51**, 635 (1969).
[28] Y. Song, E. A. Mason, and R. M. Stratt, J. Phys. Chem. **93**, 6916 (1989).
[29] M. Bishop and P. A. Whitlock, J. Chem. Phys. **123**, 014507 (2005).
[30] M. Bishop and P. A. Whitlock, J. Stat. Phys. **126**, 299 (2007).
[31] M. Bishop, N. Clisby, and P. A. Whitlock, J. Chem. Phys. **128**, 034506 (2008).
[32] G. Parisi, *Field Theory, Disorder and Simulations* (World Scientific, Singapore, 1992).
[33] F. Zamponi, "Theory of simple glasses," e-print arXiv:1212.0390v1.
[34] L. Angelani and G. Foffi, J. Phys.: Condens. Matter **19**, 256207 (2007).
[35] A. Donev, F. H. Stillinger, and S. Torquato, J. Chem. Phys. **127**, 124509 (2007); Phys. Rev. Lett. **96**, 225502 (2006).
[36] H. G. E. Hentschel, V. Ilyin, N. Makedonska, I. Procaccia, and N. Schupper, Phys. Rev. E **75**, 050404(R) (2007).
[37] B. Baeyens and H. Verschelde, Z. Phys. B: Condens. Matter **102**, 255 (1997); J. Math. Phys. **36**, 201 (1995).
[38] K. Ball, Int. Math. Res. Notices **1992**, 217 (1992).
[39] H. Cohn, Geom. Topol. **6**, 329 (2002); H. Cohn and N. Elkies, Ann. Math. **157**, 689 (2003).
[40] S. Torquato and F. H. Stillinger, Exp. Math. **15**(3), 307 (2006); A. Scardicchio, F. H. Stillinger, and S. Torquato, J. Math. Phys. **49**, 043301 (2008).
[41] S. Auer and D. Frenkel, Nature (London) **409**, 1020 (2001).
[42] R. P. Sear, Europhys. Lett. **44**, 531 (1998).
[43] P. N. Pusey, E. Zaccarelli, C. Valeriani, E. Sanz, W. C. K. Poon, and M. E. Cates, Philos. Trans. R. Soc. London, Ser. A **367**, 4993 (2009).
[44] J. Kolafa, S. Labik, and A. Malijevsky, Phys. Chem. Chem. Phys. **6**, 2335 (2004); D. Ayala de Lonngi and P. Alejandro Lonngi Villanueva, Mol. Phys. **73**, 763 (1991).
[45] M. H. Cohen and G. S. Grest, Phys. Rev. B **20**, 1077 (1979).
[46] W. G. Hoover and F. H. Ree, J. Chem. Phys. **49**, 3609 (1968); **47**, 4873 (1967).

[47]M. Luban and A. Baram, J. Chem. Phys. **76**, 3233 (1982).
[48]H. L. Frisch and J. K. Percus, Phys. Rev. E **60**, 2942 (1999).
[49]T. Boublik, J. Chem. Phys. **53**, 471 (1970); G. A. Mansoori, N. F. Carnahan, K. E. Starling, and T. W. Leland, *ibid*. **54**, 1523 (1971).
[50]A. Santos, S. B. Yuste, and M. López de Haro, J. Chem. Phys. **135**, 181102 (2011).
[51]F. H. Stillinger, P. G. Debenedetti, and T. M. Truskett, J. Phys. Chem. B **105**, 11809 (2001).
[52]C. A. Rogers, *Packing and Covering* (Cambridge University Press, Cambridge, 1964); J. H. Conway and N. J. A. Sloane, *Sphere Packings, Lattices and Groups* (Spriger-Verlag, New York, 1993).
[53]S. Torquato, O. U. Uche, and F. H. Stillinger, Phys. Rev. E **74**, 061308 (2006).
[54]H. Reiss, H. L. Frisch, and J. L. Lebowitz, J. Chem. Phys. **31**, 369 (1959).
[55]R. Jadrich and K. S. Schweizer, J. Chem. Phys. **139**, 054502 (2013).